A Generalized Framework Model for the Simulation of Gas Production in Unconventional Gas Reservoirs

Yu-Shu Wu, SPE, Colorado School of Mines; **Jianfang Li,** SPE, Research Institute of Petroleum Exploration and Development; **Didier-Yu Ding,** SPE, IFP Energies Nouvelles; **Cong Wang,** SPE, Colorado School of Mines; and **Yuan Di,** Peking University

Summary

Unconventional gas resources from tight-sand and shale gas reservoirs have received great attention in the past decade around the world because of their large reserves and technical advances in developing these resources. As a result of improved horizontal-drilling and hydraulic-fracturing technologies, progress is being made toward commercial gas production from such reservoirs, as demonstrated in the US. However, understandings and technologies needed for the effective development of unconventional reservoirs are far behind the industry needs (e.g., gas-recovery rates from those unconventional resources remain very low). There are some efforts in the literature on how to model gas flow in shale gas reservoirs by use of various approaches—from modified commercial simulators to simplified analytical solutions—leading to limited success. Compared with conventional reservoirs, gas flow in ultralow-permeability unconventional reservoirs is subject to more nonlinear, coupled processes, including nonlinear adsorption/desorption, non-Darcy flow (at both high flow rate and low flow rate), strong rock/fluid interaction, and rock deformation within nanopores or microfractures, coexisting with complex flow geometry and multiscaled heterogeneity. Therefore, quantifying flow in unconventional gas reservoirs has been a significant challenge, and the traditional representative-elementary-volume- (REV) based Darcy's law, for example, may not be generally applicable.

In this paper, we discuss a generalized mathematical framework model and numerical approach for unconventional-gas-reservoir simulation. We present a unified framework model able to incorporate known mechanisms and processes for two-phase gas flow and transport in shale gas or tight gas formations. The model and numerical scheme are based on generalized flow models with unstructured grids. We discuss the numerical implementation of the mathematical model and show results of our model-verification effort. Specifically, we discuss a multidomain, multicontinuum concept for handling multiscaled heterogeneity and fractures [i.e., the use of hybrid modeling approaches to describe different types and scales of fractures or heterogeneous pores—from the explicit modeling of hydraulic fractures and the fracture network in stimulated reservoir volume (SRV) to distributed natural fractures, microfractures, and tight matrix]. We demonstrate model application to quantify hydraulic fractures and transient flow behavior in shale gas reservoirs.

Introduction

Even with the significant progress made in producing natural gas from unconventional, low-permeability shale gas and tight gas reservoirs in the past decade, gas recovery remains very low (estimated at 10 to 30% of gas in place). Gas production or flow in such extremely low-permeability formations is complicated further by many coexisting processes, such as severe heterogeneity, a large Klinkenberg effect (Klinkenberg 1941), nonlinear or non-Darcy flow behavior, adsorption/desorption, strong interactions between fluid (gas and water) molecules, and solid materials within tiny pores, as well as micro- and macrofractures of shale and tight formations. Currently, there is little in basic understanding of how these complicated flow behaviors impact gas flow and the ultimate gas recovery in such reservoirs. In particular, only a few effective reservoir simulators and few modeling studies currently are available (e.g., Kelkar and Atiq 2010) in the industry for assisting reservoir engineers to model and develop the unconventional natural-gas resources.

Shale formations are characterized by extremely low permeability from subnanodarcies to microdarcies, and it is different for different shale types, even under similar porosity, stress, or pore pressure. As summarized by Wang et al. (2009), the permeability of deep organic-lean mudrocks ranges from smaller than to tens of nanodarcies, whereas permeability values in organic-rich gas shales range from subnanodarcies to tens of microdarcies. The Klinkenberg effect (Klinkenberg 1941), or gas-slippage effect, has been practically ignored in conventional gas reservoir studies, except when analyzing pressure responses or flow near gas-production wells at a very low pressure. This is because of a larger pore size and relatively high pressure existing in those conventional gas reservoirs. In shale gas reservoirs, however, the Klinkenberg or slippage effect is expected to be significant because of the nanosized pores of such rock, even under a high-pressure condition. Wang et al. (2009) show that gas permeability in the Marcellus shale increases from 19.6 μd at 1,000 psi to 54 μd at 80 psi because of the strong slippage effect.

Unconventional reservoir dynamics are characterized by the highly nonlinear behavior of multiphase flow in extremely low-permeability rock, coupled by many coexisting physical processes (e.g., non-Darcy flow). Because of complicated flow behavior, a strong interaction between fluid and rock, and multiscaled heterogeneity, the traditional Darcy's-law/REV-based model may not be generally applicable for describing flow phenomena in unconventional gas reservoirs. Blasingame (2008) and Moridis et al. (2010) provide very comprehensive reviews of flow mechanisms in unconventional shale gas reservoirs. Both studies point out that the nonlaminar/non-Darcy flow concept of high velocity may turn out to be important in shale gas production. The nonlaminar/non-Darcy flow concept of high-velocity flow in shale gas reservoirs may not be represented by Darcy's law, and the Forchheimer equation is probably sufficient for many applications.

Natural gas in shale gas formations is present both as a free-gas phase and as gas adsorbed onto solids in pores. In these reservoirs, gas or methane molecules are adsorbed mainly to the carbon-rich components (i.e., kerogen) (Silin and Kneafsey 2011; Mengal and Wattenbarger 2011; EIA 2011). The adsorbed gas represents a significant percentage of total gas reserves (20 to 80%) as well as a significant factor in recovery rates, which cannot be ignored in any model or modeling analysis. In shale gas formations, past studies found that methane molecules are adsorbed mainly to the carbon-rich components (i.e., kerogen), correlated with total organic content (TOC) in shales, as a function of reservoir pressure.

In conventional oil or gas reservoirs, the effect of geomechanics on rock deformation or permeability is generally small

This paper (SPE 163609) was accepted for presentation at the SPE Reservoir Simulation Symposium, The Woodlands, Texas, USA, 18–20 February 2013, and revised for publication. Original manuscript received for review 4 March 2013. Revised manuscript received for review 13 January 2014. Paper peer approved 5 February 2014.

and has been mostly ignored in practice. However, in unconventional shale formations with nanosized pores or nanosized microfractures, such geomechanics effects can be relatively large and may have a significant impact on both fracture and matrix permeability, which has to be considered, in general. Wang et al. (2009) show that permeability in the Marcellus shale is pressure-dependent and decreases with an increase in the confining pressure (or total stress). The effect of confining pressure on permeability is caused by a reduction of porosity. Bustin et al. (2008) report the effect of stress (confining pressure) in Barnett, Muskwa, Ohio, and Woodford shales and show that the degree of permeability reduction with confining pressure is significantly higher in shales than in consolidated sandstone or carbonate.

This paper presents a generalized mathematical model and numerical approach for unconventional-gas-reservoir simulation. We present a unified framework model that is able to incorporate many known mechanisms and processes for two-phase gas flow in shale gas or tight gas formations with a continuum modeling approach. The numerical scheme is based on generalized flow models with unstructured grids. We discuss the numerical implementation of Klinkenberg effects, non-Darcy flow, gas adsorption, and geomechanics effects into the mathematical model. In the numerical-modeling examples, we apply geomechanics-coupled permeability to fractures, and apply the Klinkenberg effect to matrix media. This is because the Klinkenberg effect is apparent with extremely low permeability or tiny pores, whereas fractures are very sensitive to the change in effective stress. Results of our model-verification effort are also presented. We demonstrate model application to quantify hydraulic fractures and transient flow behavior in shale gas reservoirs.

One of the critical issues in shale-gas-reservoir simulation is how to handle fracture flow and fracture/matrix interaction. This is because the gas flow and production rely on fractures in these reservoirs. Cipolla et al. (2009) built a methodology on modeling complex fracture geometry and heterogeneity from the microseismic data. In this paper, we present a hybrid fracture-modeling approach, defined as a combination of explicit fracture modeling and multicontinuum, multiple-interacting-continua (MINC) (Pruess and Narasimhan 1985), and single-porosity modeling approaches, which seems the best option for modeling a shale gas reservoir with both hydraulic fractures and natural fractures. This is because hydraulic fractures, which have to be dealt with for shale gas production, are better handled by the explicit fracture method but cannot be modeled, in general, by a dual-continuum model. On the other hand, naturally fractured reservoirs are better modeled by a dual-continuum approach, such MINC, for extremely low-permeability matrix in shale gas formations, which cannot be modeled by an explicit fracture model. Specifically, we demonstrate how to use the hybrid modeling approach to describe different types and scales of fractures from the explicit modeling of hydraulic fractures and fracture network in the SRV to distributed natural fractures, microfractures, and tight matrix.

Flow-Governing Equations

In most cases of gas production from shale gas formations, a two-phase (gas/liquid) -flow model or a multiphase-flow model is considered to be sufficient for simulation studies. This is because what we are most concerned with in shale-gas-reservoir simulation is the modeling of gas flow from reservoir to well. However, in addition to the gas phase, liquid-phase flow is often occurring simultaneously with gas flow; it needs to be considered when two cases exist—mobile in-situ connate water and an abundance of aqueous hydraulic-fracturing fluids, which are sucked into the formations surrounding the wells. Therefore, in this paper, we primarily discuss the two-phase (gas and liquid) -flow model and formulation and treat single-phase gas flow as a special case of the two-phase flow for the simulation studies of unconventional gas reservoirs.

A multiphase system of gas and water (or liquid) in a porous or fractured unconventional reservoir is assumed to be similar to what is described in a black-oil model, composed of two phases: gaseous and aqueous. For simplicity, the gas and water components are assumed to be present only in their associated phases and adsorbed gas is within the solid phase of rock. Each fluid phase flows in response to pressure and gravitational and capillary forces according to the multiphase extension of Darcy's law or several extended non-Darcy-flow laws, discussed next. In an isothermal system containing two mass components, subject to multiphase flow and adsorption, two mass-balance equations are needed to fully describe the system, as described in an arbitrary flow region of a porous or fractured domain for flow of phase β ($\beta = g$ for gas and $\beta = w$ for water),

$$\frac{\partial}{\partial t}(\phi S_\beta \rho_\beta + m_\beta) = -\nabla \cdot (\rho_\beta v_\beta) + q_\beta. \quad \ldots\ldots\ldots\ldots \quad (1)$$

where ϕ is the effective porosity of the porous or fractured media; S_β is the saturation of fluid β; ρ_β is the density of fluid β; v_β is the volumetric velocity vector of fluid β, determined by Darcy's law or non-Darcy-flow models, discussed next; t is time; m_β is the adsorption or desorption mass term for the gas component per unit volume of formation; and q_β is the sink/source term of phase (component) β per unit volume of formation.

Incorporation of Gas Adsorption and Desorption. The amount of adsorbed gas in a given shale gas formation is generally described with the Langmuir's isotherm (e.g., Moridis et al. 2010; Mengal and Wattenbarger 2011; Silin and Kneafsey 2011; EIA 2011; Wu et al. 2012; Wu and Wang 2012) (i.e., it is correlated to reservoir gas pressure). To incorporate the gas adsorption or desorption mass term in the mass-conservation equation, the amount of adsorbed gas is determined according to the Langmuir's isotherm as a function of reservoir pressure. As the pressure decreases with continuous gas production through production wells in reservoirs, more adsorbed gas is released from the solid to the free-gas phase in the pressure-lowering region, contributing to the total gas flow or production. In our model, the mass of adsorbed gas in unit formation volume is described (Leahy-Dios et al. 2011; Silin and Kneafsey 2011; Wu et al. 2012) as

$$m_g = \rho_R \rho_g V_E, \quad \ldots\ldots\ldots\ldots \quad (2)$$

where m_g is adsorbed gas mass in unit formation volume; ρ_R is rock bulk density; ρ_g is gas density at standard condition; and V_E is the adsorption isotherm function or gas content in scf/ton (or standard gas volume adsorbed per unit rock mass). If the adsorbed-gas terms can be represented by the Langmuir isotherm (Langmuir 1916), the dependency of adsorbed-gas volume on pressure at constant temperature is given as

$$V_E = V_L \frac{P}{P + P_L}, \quad \ldots\ldots\ldots\ldots \quad (3)$$

where V_L is the Langmuir's volume in scf/ton; P is reservoir gas pressure; and P_L is Langmuir's pressure, the pressure at which 50% of the gas is desorbed. In general, Langmuir's volume V_L is a function of the organic richness (or TOC) and thermal maturity of the shale.

Note that Eq. 3 is valid only for the case when the Langmuir model is applicable. In general, V_E in Eq. 2 can be determined from any correlation of gas adsorption as a function of reservoir gas pressure, which may be defined by a table lookup from laboratory studies for a given unconventional reservoir.

In the literature, the most commonly used empirical model describing sorption onto organic carbon in shales is analogous to that used in coalbed methane and follows the Langmuir isotherm (Gao et al. 1994; Moridis et al. 2010), such as Eq. 2. This adsorption-modeling approach is based on the assumption that an instantaneous equilibrium exists between the sorbed and the free gas (i.e., there is no transient-time lag between pressure changes and the corresponding sorption/desorption responses; i.e., the equilibrium model of the Langmuir sorption is assumed to be valid, which provides a good approximation in shale gas modeling).

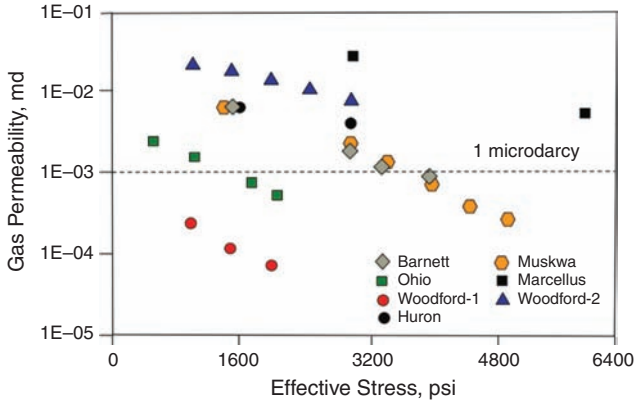

Fig. 1—Effect of confining pressure on gas permeability in gas shales (Wang et al. 2009).

Several kinetic sorption models exist in the literature that use diffusion approaches; however, the subject has not been fully investigated or fully understood (Moridis et al. 2010).

Coupled Flow and Geomechanics Effect. In this section, we will propose a simple-to-implement modeling approach, easy to incorporate into an existing reservoir simulator, to couple geomechanics with two-phase flow in unconventional reservoirs. The following discussion is based on our previous work (e.g., Wu et al. 2008; Winterfeld and Wu 2011). The effective porosity, permeability, and capillary pressure of rock are assumed to correlate with the mean effective stress (σ'_m), defined as

$$\sigma'_m = \sigma(x, y, z, P) - \alpha P, \quad \ldots \quad (4)$$

where α is the Biot constant and

$$\sigma_m(x, y, z, P) = [\sigma_x(x, y, z, P) + \sigma_y(x, y, z, P) + \sigma_z(x, y, z, P)]/3, \quad \ldots \quad (5)$$

where σ_x, σ_y, and σ_z are total stress in the x-, y-, and z-direction, respectively. With the definition of the mean effective stress in Eq. 5, the effective porosity of the formation (fractures or porous media) is defined as a function of mean effective stress only,

$$\phi = \phi(\sigma'_m). \quad \ldots \quad (6)$$

Similarly, the intrinsic permeability is related to the effective stress; that is,

$$k = k(\sigma'_m). \quad \ldots \quad (7)$$

For capillary pressure functions, the impact of rock deformation or pore change is accounted for with the Leverett function (Leverett 1941),

$$P_c = C_p P_c^0(S_w) \frac{\sqrt{k^0/\phi^0}}{\sqrt{k(\sigma'_m)/\phi(\sigma'_m)}}, \quad \ldots \quad (8)$$

where P_c is the capillary pressure between gas and water as a function of water or gas saturation; C_p is a constant; and the superscript 0 denotes reference or zero-stress condition.

Several correlations have been used for porosity as a function of effective stress and permeability as a function of porosity (Davies and Davies 1999; Rutqvist et al. 2002; Winterfeld and Wu 2011, 2012). In our numerical implementation, the function for porosity and permeability presented by Rutqvist et al. (2002) is adopted, which is obtained from laboratory experiments on sedimentary rock (Davies and Davies 1999),

$$\phi = \phi_r + (\phi_0 - \phi_r)e^{-a\sigma'}, \quad \ldots \quad (9)$$

where ϕ_0 is zero-effective-stress porosity; ϕ_r is high-effective-stress porosity; and the exponent a is a parameter. Rutqvist et al. (2002), Davies and Davies (1999), and Winterfeld and Wu (2011, 2012) also present an associated function for permeability in terms of porosity,

$$k = k_o e^{c\left(\frac{\phi}{\phi_0} - 1\right)}, \quad \ldots \quad (10)$$

where c is a parameter. **Fig. 1** shows the effect of confining pressure on gas permeability in gas shales.

One can use an alternative, table-lookup approach for the correlation of reservoir porosity and permeability as a function of effective mean stress, from laboratory studies, for a given unconventional reservoir.

One must note that Fig. 1 from Wang et al. (2009) presents the permeability measurement from core plugs in which potential natural microfractures in core plugs play an important role for the connectivity. If one uses crushed samples to measure the matrix permeability only by eliminating natural and drilling induced microfactures, the permeability value is one or two orders lower. The geomechanics has a much stronger impact on the fracture than on the matrix. So, when using a dual-porosity approach in the modeling, if microfractures are considered as a part of the matrix media, one can directly apply the relations in Eqs. 4 through 10. However, if microfractures are considered as a part of the fractured media, the geomechanics effect is more complex because fracture conductivities are subjected to different laws according to microfractures, partially propped fractures, or propped fractures (Cipolla 2009).

The applicability of these mechanics-coupling models in multiphase-flow simulations for a rock-deformation effect requires that the initial distribution of effective stress or total stress field be predetermined as a function of spatial coordinates and pressure fields, as in Eq. 5. In practice, the stress distribution may be estimated analytically, numerically, or from field measurements because changes in effective stress are primarily caused by changes in reservoir pressure during production. These models can be significantly simplified for coupling multiphase gas flow with rock deformation in stress-sensitive formations in numerical simulation, if the in-situ total stress in reservoirs is nearly constant or a function of spatial coordinates as well as fluid pressure only during the production. The constant-total-stress requirement may be approximately satisfied for deep reservoirs.

Incorporation of Klinkenberg or Gas-Slippage Effect. In low-permeability shale gas formations with nanosized pores or under a low-reservoir-pressure condition, the Klinkenberg effect (Klinkenberg 1941) may be significant and should be accounted for when modeling gas flow in such reservoirs (Wu et al. 1998; Wang et al. 2009). As discussed previously, the Klinkenberg effect is expected to be larger or stronger in unconventional reservoirs because of small pore size and low permeability in comparison with those in conventional reservoirs. The Klinkenberg effect, if existing, will enhance gas permeability or productivity in a low-pressure zone, such as the region near a well or matrix portions near fractures, of low-permeability unconventional formations, and, therefore, it should be included as an additional beneficial factor of gas-flow enhancement.

The Klinkenberg effect is incorporated in gas-flow models by modifying absolute permeability for the gas phase as a function of gas pressure (e.g., Wu et al. 1998),

$$k_g = k_\infty \left(1 + \frac{b}{P_g}\right), \quad \ldots \quad (11)$$

where k_∞ is constant, absolute gas-phase permeability under very large gas-phase pressure (in which the Klinkenberg effect is minimized); and b is the Klinkenberg beta factor and could be pressure- or temperature-dependent, accounting for the gas-slippage effect.

In a conventional-gas-reservoir simulation, the beta factor is commonly treated as constant and depends on the pore structure of the medium and formation temperature for a particular reservoir. Several recent studies on dynamic gas slippage with

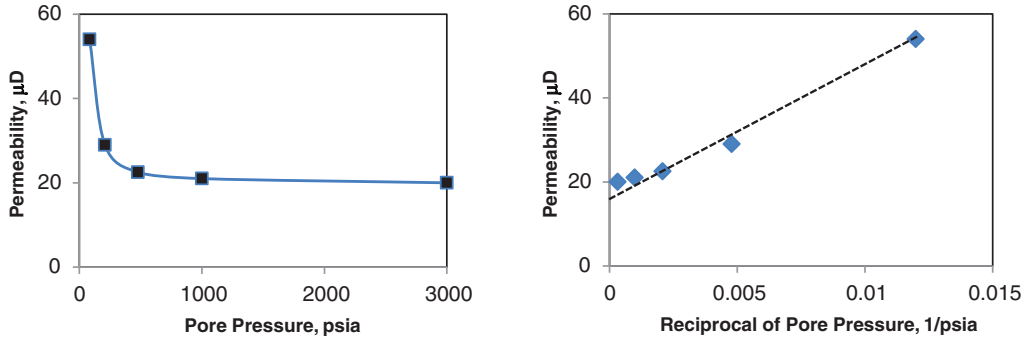

Fig. 2—Contribution of the Klinkenberg effect to the apparent matrix permeability (Ozkan et al. 2010).

microscale or pore-scale models have considered the beta factor as a function of gas pressure or the Knudsen number. In application, the Klinkenberg effect should be modeled with the laboratory-determined beta factor either as a constant or as a pressure-dependent function or simply treating the apparent gas permeability as a function of pressure from a table lookup to include the Klinkenberg effect or the Knudsen diffusion. An example relation between permeability and pressure, as shown in **Fig. 2**, can be directly used for the reservoirs concerned, if a site-specific study provides such correlations or plots.

After a comparison of Fig. 1 and **Fig. 3,** the Klinkenberg effect seems to have less impact than that of geomechanics, and they are going in the opposite directions. Geomechanics has an effect mainly on the microfractures and stimulation fractures, whereas the Klinkenberg effect is primarily on the matrix media with nanosized pores or fractures.

A dynamic gas-slippage theory was proposed on the basis of the assumption that gas travels under the influence of a concentration field (random molecular flow) and a pressure field (macroscopic flow) (Ertekin et al. 1986). According to this theory, the Klinkenberg factor is not a constant anymore, but a pressure-dependent value. They gave the expression of the Klinkenberg factor as

$$b = \frac{P c_g D_g \mu}{k_g}, \quad \ldots\ldots\ldots\ldots\ldots\ldots\ldots\ldots \quad (12)$$

where c_g is gas compressibility and D is diffusivity coefficient.

In Eq. 12, the correlation to compute the diffusivity constant is given by Ertekin et al. (1986):

$$D_g = \frac{31.57}{\sqrt{M_g}} k^{0.67}, \quad \ldots\ldots\ldots\ldots\ldots\ldots\ldots\ldots \quad (13)$$

where D_g is in ft^2/D.

We analyze the Klinkenberg effect with three different matrix permeabilities—1.0×10^{-3}md, 1.0×10^{-5}md, and 1.0×10^{-7} md, as shown in Fig. 2 and **Fig. 4.** We can see that the contribution of the Klinkenberg effect is more significant at low pressures and for lower values of permeability. This estimation also provides reliable values of the beta factor for analyzing the Klinkenberg effect.

The Incorporation of NonDarcy Gas Flow. In addition to multiphase Darcy flow, non-Darcy flow may also occur between and among the continua, such as along fractures, in unconventional gas reservoirs. The flow velocity, $\mathbf{v}_\beta$, for the non-Darcy flow of each fluid may be described with the multiphase extension of the Forchheimer equation (e.g., Wu 2002),

$$-(\nabla \Phi_\beta) = \frac{\mu_\beta}{k \cdot k_{r\beta}} \mathbf{v}_\beta + \beta_\beta \rho_\beta \mathbf{v}_\beta |\mathbf{v}_\beta|, \quad \ldots\ldots\ldots\ldots \quad (14)$$

where β_β is presented the effective non-Darcy-flow coefficient with a unit m^{-1} for fluid β under multiphase-flow conditions. The correlation proposed by Evans and Civan is used to determine the non-Darcy-flow beta factor in the Forchheimer equation (Evans and Civan 1994) in our simulation examples, such as

$$\beta = \frac{1.485 \times 10^9}{k^{1.021}}, \quad \ldots\ldots\ldots\ldots\ldots\ldots\ldots\ldots \quad (15)$$

where the unit of k is md and the unit of β is ft^{-1}. This correlation for β matched with more than 180 data points, including those for propped fractures (correlation coefficient = 0.974).

Numerical Model

As discussed previously, the partial-differential equation that governs gas and liquid flow in shale gas reservoirs is nonlinear. In addition, gas flow in unconventional reservoirs is subject to many

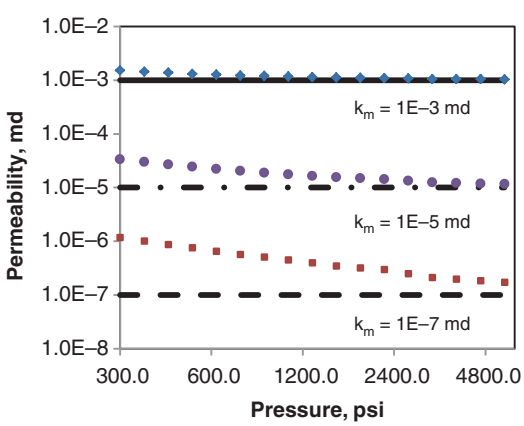

Fig. 3—Effect of pore pressure on gas permeability in the Marcellus shale, with a confining pressure of 3,000 psi (Soeder 1988; Wang et al. 2009).

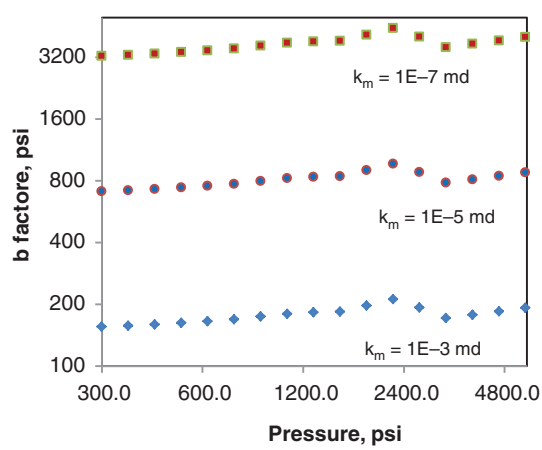

Fig. 4—Estimations of Klinkenberg beta factor for three permeability values.

other nonlinear flow processes, such as adsorption and non-Darcy flow. In general, the flow model needs to be solved with a numerical approach. This work follows the methodology for reservoir simulation (i.e., the use of numerical approaches to simulate gas and water flow), following three steps: (1) spatial discretization of mass-conservation equations; (2) time discretization; and (3) iterative approaches to solve the resulting nonlinear, discrete algebraic equations.

Discrete Equations. The component mass-balance equations (Eq. 1) are discretized in space with a control-volume or integrated finite-difference concept (Pruess et at. 1999). The control-volume approach provides a general spatial discretization scheme that can represent a 1D, 2D, or 3D domain with a set of discrete meshes. Each mesh has a certain control volume for a proper averaging or interpolation of flow and transport properties or thermodynamic variables. Time discretization is carried out with a backward, first-order, fully implicit finite-difference scheme. The discrete nonlinear equations for components of gas and water at gridblock or node i can be written in a general form:

$$\left[(\phi\rho S)_i^{\beta,n+1} + m_i^{\beta,n+1} - (\phi\rho S)_i^{\beta,n} - m_i^{\beta,n}\right]\frac{V_i}{\Delta t} = \sum_{j\in\eta_i} \text{flow}_{ij}^{\beta,n+1} + Q_i^{\beta,n+1}$$
$$(\beta = \text{gas and liquid}) \text{ and } (i = 1,2,3,\ldots,N), \quad (16)$$

where superscript β serves also as an equation index for gas and water components, with $\beta = 1$ (gas) and $\beta = 2$ (water); superscript n denotes the previous time level, with $n+1$ as the current time level to be solved; subscript i refers to the index of gridblock or node i, with N as the total number of nodes in the grid; Δt is time-step size; V_i is the volume of node i; η_i contains the set of direct neighboring nodes (j) of node i; and m_i^k, $flow_{ij}^k$, and Q_i^k are the adsorption or desorption, the component mass "flow" term between nodes i and j, and sink/source term at node i for component k, respectively.

Eq. 16 presents a precise form of the balance equation for each mass component of gas and water in a discrete form. It states that the rate of change in mass accumulation (plus adsorption or desorption, if existing) at a node over a timestep is exactly balanced by an inflow/outflow of mass and also by sink/source terms, when existing for the node. As long as all flow terms have the flow from node i to node j equal to and opposite to that of node j to node i for fluids, no mass will be lost or created in the formulation during the solution. Therefore, the discretization in Eq. 16 is conservative.

The "flow" terms in Eq. 16 are mass fluxes by advective processes and are described, when Darcy's law is applicable, by a discrete version of Darcy's law; that is, the mass flux of fluid phase β along the connection is given by

$$flow_{ij}^{\beta} = \lambda_{\beta,ij+1/2}\gamma_{ij}(\Phi_{\beta j} - \Phi_{\beta i}), \quad (17)$$

where $\lambda_{\beta,i\,j+1/2}$ is the mobility term to phase β, defined as

$$\lambda_{\beta,ij+1/2} = \left(\frac{\rho_\beta k_{r\beta}}{\mu_\beta}\right)_{ij+1/2}. \quad (18)$$

In Eq. 17, γ_{ij} is transmissivity and is defined, for a Voronoi grid, as (Pruess et al. 1999)

$$\gamma_{ij} = \frac{A_{ij}k_{ij+1/2}}{D_i + D_j}, \quad (19)$$

where A_{ij} is the common interface area between the connected blocks or nodes i and j; D_i is the distance from the center of block i to the common interface of blocks i and j; and $k_{ij+1/2}$ is an averaged (such as harmonic-weighted) absolute permeability along the connection between elements i and j.

In this numerical approach, we apply the upstream weighting method to the mobility term and the harmonic mean method to the transmissivity term to guarantee the convergence and accuracy of the calculation. The flow-potential term in Eq. 17 is defined as

$$\Phi_{\beta j} = P_{\beta i} - \rho_{\beta,ij+1/2} g Z_i, \quad (20)$$

where Z_i is the depth to the center of block i from a reference datum.

Handling the Klinkenberg Effect. To include the Klinkenberg effect on gas flow, the absolute permeability to gas phase in Eq. 19 should be evaluated with Eq. 11 as a function of gas-phase pressure.

Handling the Non-Darcy Flow. Under the non-Darcy-flow condition of Eq. 14, the flow term ($\text{flow}_{\beta ij}$) in Eq. 17 along the connection (i, j), between elements i and j, is numerically defined as (Wu 2002)

$$flow_{\beta,ij} = \frac{A_{ij}}{2(k\beta_\beta)_{ij+1/2}}\left\{-\frac{1}{\lambda_\beta} + \left[\left(\frac{1}{\lambda_\beta}\right)^2 - \overline{\gamma}_{ij}(\Phi_{\beta j} - \Phi_{\beta i})\right]^{1/2}\right\}, \quad (21)$$

in which the non-Darcy-flow transmissivity is defined as

$$\overline{\gamma}_{ij} = \frac{4(k^2\rho_\beta\beta_\beta)_{ij+1/2}}{D_i + D_j}. \quad (22)$$

In evaluating the "flow" terms in Eqs.17 through 22, subscript $ij + 1/2$ is used to denote a proper averaging or weighting of fluid-flow properties at the interface or along the connection between two blocks or nodes i and j. For example, we use upstream weighting for relative permeability, density, and non-Darcy coefficient. The convention for the signs of flow terms is that flow from node j into node i is defined as "+" (positive) in calculating the flow terms.

Handling Fractured Media. Handling flow through fractured media is critical in shale-gas-reservoir simulation, because gas production from such low-permeability formations relies on fractures, from hydraulic-fracture networks to various-scaled natural fractures, to provide flow channels for gas flow into producing wells. Therefore, any unconventional reservoir simulator must have the capability of handling fractured media. The published modeling exercises in the literature have paid much attention to modeling fractures in shale gas formations (e.g., Cipolla 2009; Freeman et al. 2009a,2009b; 2010; Moridis et al. 2010; Cipolla et al. 2010; Rubin 2010; Li et al. 2011; Wu et al. 2012). However, note that very few studies have been carried out to address the critical issues as how to accurately simulate fractured unconventional gas reservoirs or to select the best approach for modeling a given shale gas formation. Most of the modeling exercises use commercial reservoir simulators, developed for conventional-fractured-reservoir simulation, which have very limited capabilities for modeling multiscaled or complicated fractured reservoirs. On the other hand, to simulate fractured unconventional gas reservoirs, more effort on model development is needed—from new conceptual models to in-depth modeling studies of laboratory to field-scale application.

In our opinion, the hybrid fracture-modeling approach—defined as a combination of explicit fracture modeling (discrete-fracture model) and MINC (Pruess and Narasimham 1985; Pruess 1983) and single-porosity modeling approaches—provides the best option for modeling a shale gas reservoir with both hydraulic fractures and natural fractures. This is because hydraulic fractures, which have to be dealt with for shale gas production, are better handled by the explicit fracture method, and they cannot be

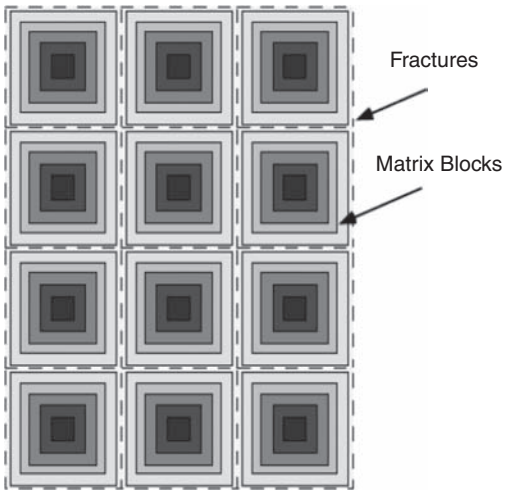

Fig. 5—Schematic of MINC concept (Pruess and Narasimham 1985).

modeled, in general, by a dual-continuum model. On the other hand, naturally fractured reservoirs are better modeled by a dual-continuum approach, such as MINC, for extremely low-permeability matrix in shale gas formations, which cannot be modeled by an explicit-fracture model.

An explicit-fracture-modeling, or discrete-fracture, concept is to include every fracture explicitly in the modeled system by the use of refined grids to discretize fractures and the matrix surrounding fractures. This approach is a good option for simulating hydraulic fractures for gas production from hydraulic-fractured wells in a nonfractured/shale gas reservoir. The advantage of this approach is that it can model hydraulic fractures accurately when the fractures are known for their spatial distributions, determined from other fracture-characterization studies. The disadvantage is that it cannot be used for simulating natural fractures or microfractures, in general, because the number of natural fractures or microfractures in a shale gas reservoir is too large for the model to handle and their actual distributions in formations are unknown.

For the low matrix permeability or large matrix-block size, the traditional double-porosity model may not be applicable for modeling natural fractures in unconventional reservoirs. This is because it takes years to reach the pseudosteady state under which the double-porosity model applies. The MINC concept (Pruess and Narasimham 1985) is able to describe gradients of pressures, temperatures, or concentrations near the matrix surface and inside the matrix—by further subdividing individual matrix blocks with 1D or multidimensional strings of nested meshes, as shown in **Fig. 5.** Therefore, the MINC method treats interporosity flow in a fully transient manner by computing the gradients that drive interporosity flow at the matrix/fracture interface. In comparison with the double-porosity or dual-permeability model, MINC does not rely on the pseudosteady-state assumption to calculate fracture/matrix flow and is able to simulate fully transient fracture/matrix interaction by subdividing nested-cell gridding inside matrix blocks. The MINC concept should be generally applicable for handling fracture/matrix flow in fractured-shale gas reservoirs, no matter how large the matrix-block size is or how low the matrix permeability is, and it is more suitable for handling fractured-shale gas reservoirs. However, the MINC approach may not be applicable to systems in which fracturing is so sparse that the fractures cannot be approximated as a continuum.

As **Fig. 6** shows, in our hybrid fracture model, both the hydraulic fractures and SRV are evaluated from the microseismic cloud. Recent advances in microseismic-fracture mapping technology have provided previously unavailable information to characterize hydraulic-fracture growth and SRV, and have documented surprising complexities in many geological environments. We will have a primary hydraulic-fracture system and an associated stimulated volume in each hydraulic-fracture stage. First, we define a primary fracture on the basis of the orientation and region of the microseismic cloud. The hydraulic fractures are modeled by the discrete-fracture method. We assume the SRV near the hydraulic fractures is the region with natural fractures, and we apply MINC in this region. Single-porosity is applied in the region outside the SRV, in which there are no natural fractures. Local grid refinement (LGR) is used to improve simulation accuracy because pressure gradients change substantially over short distances in the regions near hydraulic fractures. LGR is performed near the hydraulic-fracture region.

Numerical Solution. In this work, we use the fully implicit scheme to solve the discrete nonlinear Eq. 16 with a Newton iteration method. Let us write the discrete nonlinear equation, Eq. 16, in a residual form as

$$R_i^{\beta,n+1} = \left[(\phi\rho S)_i^{\beta,n+1} + m_i^{\beta,n+1} - (\phi\rho S)_i^{\beta,n} - m_i^{\beta,n}\right]\frac{V_i}{\Delta t} - \sum_{j\in\eta_i} \text{flow}_{ij}^{\beta,n+1} - Q_i^{\beta,n+1} = 0$$
$$(\beta = 1,2;\quad i = 1,2,3,\ldots,N). \qquad (23)$$

Eq. 23 defines a set of $2\times N$ coupled nonlinear equations that need to be solved for every balance equation of mass components, respectively. In general, two primary variables per node are needed to use the Newton iteration for the associated two equations per node. The primary variables selected are gas pressure

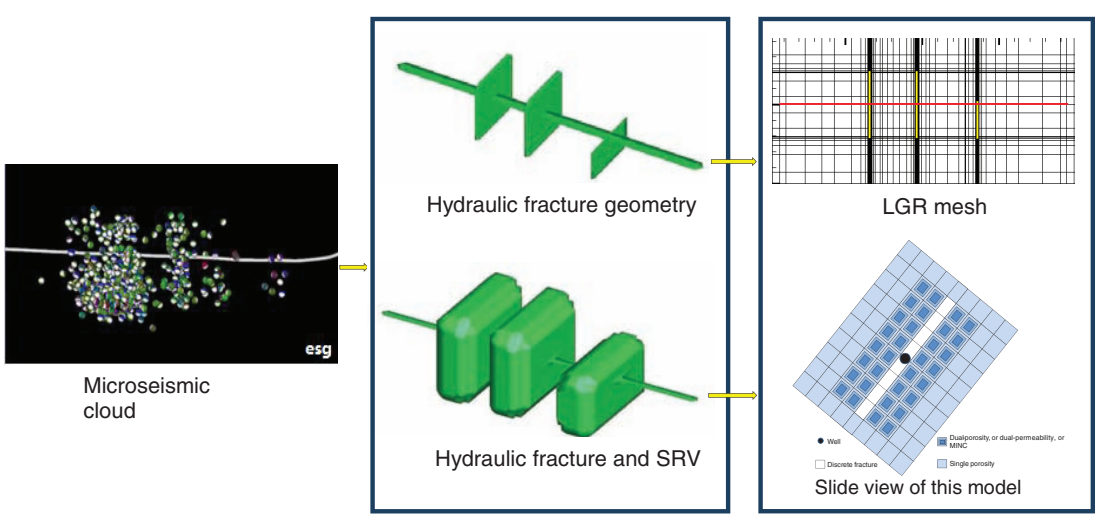

Fig. 6—Hybrid fracture model built methodology from microseismic cloud.

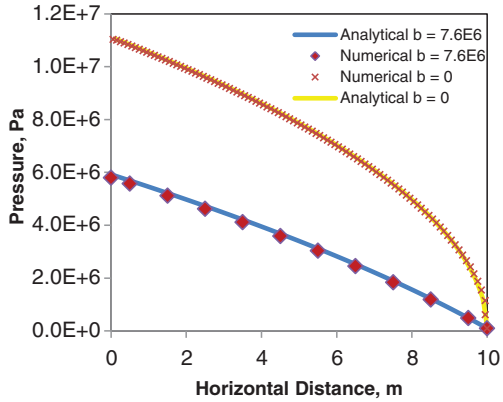

Fig. 7—Analytical and numerical results for linear flow with the Klinkenberg effect.

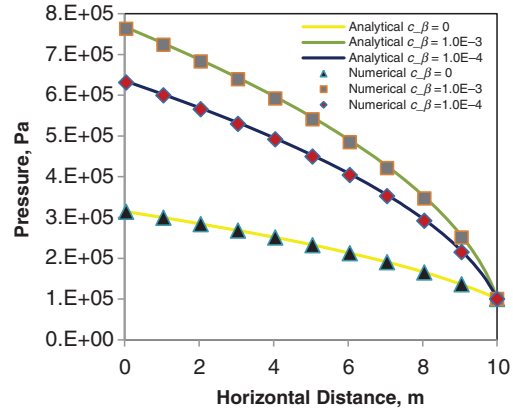

Fig. 8—Analytical and numerical results for linear non-Darcy flow.

and gas saturation. The rest of the dependent variables—such as relative permeability, capillary pressures, viscosity and densities, adsorption term, and nonselected pressure and saturation—are treated as secondary variables, which are calculated from selected primary variables.

In terms of the primary variables, the residual equation, Eq. 23, at a node i is regarded as a function of the primary variables at not only node i, but also at all its direct neighboring nodes j. The Newton iteration scheme gives rise to

$$\sum_m \frac{\partial R_i^{\beta,n+1}(x_{m,p})}{\partial x_m}(\delta x_{m,p+1}) = -R_i^{\beta,n+1}(x_{m,p}), \quad \ldots\ldots \quad (24)$$

where x_m is the primary variable m with $m = 1$ and 2, respectively, at node i and all its direct neighbors; p is the iteration level; and $i = 1, 2, 3, \ldots, N$. The primary variables in Eq. 23 need to be updated after each iteration,

$$x_{m,p+1} = x_{m,p} + \delta x_{m,p+1}. \quad \ldots\ldots\ldots\ldots\ldots\ldots\ldots \quad (25)$$

The Newton iteration process continues until the residuals $R_i^{\beta,n+1}$ or changes in the primary variables $\delta x_{m,p+1}$ over iteration are reduced below preset convergence tolerances.

Numerical methods are generally used to construct the Jacobian matrix for Eq. 24, as outlined in Forsyth et al. (1995). At each Newton iteration, Eq. 24 represents a system of $(2 \times N)$ linearized algebraic equations with sparse matrices, which are solved by a linear equation solver.

Numerical-Model Verification

To examine the accuracy of our simulator formulation in simulating porous-medium gas flow with the Klinkenberg, non-Darcy-flow, gas-adsorption, and geomechanics effects, several relevant steady and transient analytical solutions are derived or used for considering these flow mechanisms. The problem concerns steady-state and transient gas flow across a 1D reservoir. The system contains steady-/transient-state gas flow at an isothermal condition, and a constant gas mass injection/production rate is imposed at one side of the rock or well. The other boundary of the rock/reservoir is kept at constant pressure. Eventually, the system will reach steady state, if the production is maintained for a long period of time. A comparison of the pressure profiles along the rock block from the simulation and the analytical solution is shown in **Figs. 7 and 8,** indicating that our simulated pressure distribution is in excellent agreement with the analytical solutions for all the problems of 1D linear flow with the Klinkenberg or non-Darcy-flow effect.

Details about the analytical solution derivation considering the Klinkenberg and non-Darcy-flow effect are included in our previous work (Wu et al. 2012), and we will show their verification results only in this section for the 1D linear-flow steady-flow situation. Comparisons between the analytical and numerical solutions for the radial-flow and transient-flow cases are also presented in our former work. Constant coefficients for the Klinkenberg effect and correlation (Eq. 13) for the non-Darcy-flow coefficient are used with comparison results shown in Figs. 7 and 8.

Verification for Flow With Adsorption. For the gas flow with adsorption, the approximate analytical solution is given in Appendix A. The parameters used for this comparison study are porosity $\Phi = 0.15$; permeability $k = 100$ md; formation temperature $T = 25°C$; gas viscosity $\mu = 1.64 \times 10^{-2}$cp; initial pressure $P_i = 10^5$ Pa; and thickness of the radial system is 1 m. The well-boundary condition is a constant gas/mass-injection rate: $Q = 1.0 \times 10^{-4}$kg/s.

Fig. 9 presents the comparisons of the pressure profile at 1.67 days from the numerical and analytical solutions. Two situations,

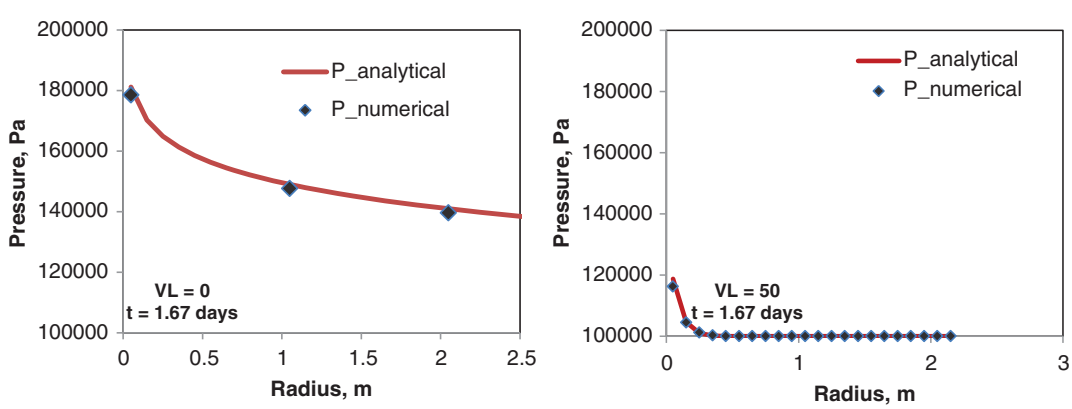

Fig. 9—Comparison of gas-pressure profiles considering gas adsorption in a radial system at 1.67 days, calculated with the numerical and analytical solutions.

TABLE 1—PARAMETERS FOR CHECKING INTEGRAL SOLUTION FOR FLOW WITH GEOMECHANICS EFFECT		
Parameter	Value	Unit
Initial pressure	$P_i = 10^7$	Pa
Initial porosity	$\Phi_i = 0.20$	
Initial fluid density	$\rho_w = 975.9$	kg/m^3
Cross-sectional area	$a = 1.0$	m^2
Formation thickness	$h = 1.0$	m
Fluid viscosity	$\mu = 0.35132 \times 10^{-3}$	$Pa \cdot s$
Fluid compressibility	$C_f = 4.556 \times 10^{-10}$	Pa^{-1}
Rock compressibility	$C_r = 5.0 \times 10^{-9}$	Pa^{-1}
Initial permeability	$k_0 = 9.860 \times 10^{-13}$	m^2
Water-injection rate	$q_m = 0.01$	kg/s
Hydraulic radius	$r_w = 0.1$	m
Exponential index	$c = 2.22$	

Langmuir volume $V_L = 0$ and $V_L = 50 m^3/kg$, are considered. The analytical solutions give an excellent match with the numerical solution.

Verification for Linear Flow With Geomechanics. Wu and Pruess (2000) presented an analytical method for analyzing the nonlinear coupled rock-permeability-variation/fluid-flow problem. Approximate analytical solutions for 1D linear and radial flow are obtained by an integral method, which is widely used in the study of steady and unsteady heat-conduction problems. The accuracy of integral solutions is generally acceptable for engineering applications. When applied to fluid-flow problems in porous media, the integral method consists of assuming a pressure profile in the pressure-disturbance zone and determining the coefficients of the profile by making use of the integral mass-balance equation.

The parameters, as shown in **Table 1,** are used to evaluate both the numerical solution and the integral solution. A comparison of injection pressures from integral and numerical solutions is shown in **Fig. 10.** The agreement between the two solutions is excellent for the entire transient period.

Model Application

In the following model-application examples, we are concerned with gas flow toward one horizontal well and a 10-stage hydraulic-fracture system in an extremely tight, uniformly porous and/or fractured reservoir **(Fig. 11).** The reservoir formation is at liquid/gas, two-phase condition; however, the liquid saturation is set at residual values as an immobile phase. This is a single-phase gas-flow problem and is modeled by the two-phase-flow reservoir simulator. The immobile liquid flow is controlled by liquid relative permeability curves.

We demonstrate the application of the proposed mathematical model for modeling gas production from a producer with 10-stage hydraulic fracturing in a shale gas reservoir. The stress alteration induced by hydraulic fracturing may activate existing natural fractures, and therefore opens microflow channels in the drainage area of the stimulated well. Here, we present the simulation of a hydraulic-fracturing problem as an example case to illustrate the capability of our hybrid fracture model to capture such a complex fracture network in these reservoirs. Three different fracture models (as shown in **Fig. 12**) are built, and their flow behavior is compared. The first one considers that there is no natural-fracture-active area, and the whole formation is single-porosity shales with low permeability. In the second model, we assume that only the natural fractures within the SRV near the hydraulic fractures are active and the rest of the natural fractures outside the SRV remain inactive. An increase in pore pressure around the hydraulic fracture causes a significant reduction in the effective stresses, potentially reopening the existing healed natural fractures or creating new fractures. As a result, the permeability near the well of the reservoir is significantly improved. This effect would help increase the well productivity in the initial production. The third fracture model is that all the formation is naturally fractured.

To simulate the performance of this system with our model, hydraulic fractures are represented by the discrete-fracture model and an active, naturally fractured reservoir area is described by the multicontinuum-fracture model, whereas a nonactive-natural-fracture reservoir area is represented by the single-porosity model. The basic parameter set for the simulation and discussion is summarized in **Table 2,** which are chosen field data.

We first compare the gas-production behavior for these three fracture models. Then, on the basis of the second fracture model (i.e., reactivated natural fractures only in SRV), we analyze the cumulative-gas-production curves with the Klinkenberg, geomechanics, and adsorption/desorption effects.

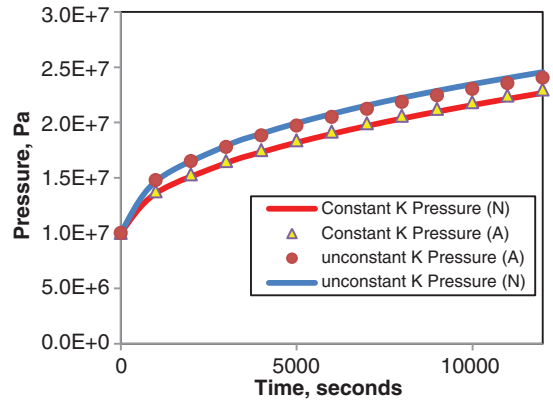

Fig. 10—Comparison of injection pressures calculated from integral and numerical solutions for linear flow in a permeability-dependent medium with constant and nonconstant permeability function.

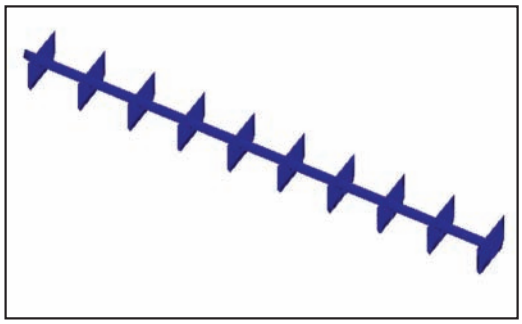

Fig. 11—Horizontal and multistaged hydraulic-fracture model.

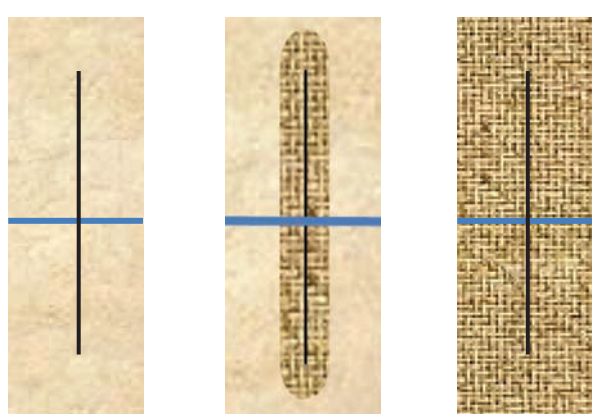

Fig. 12—Three different fracture models: From left to right are no-natural-fracture model, SRV model, and all-formation-naturally-fractured model.

TABLE 2—DATA USED FOR THE CASE STUDIES

Reservoir length, Δx, ft	5,500	Hydraulic-fracture permeability, k_{hf}, md	1×10^{5}
Reservoir width, Δy, ft	2,000	Natural-fracture porosity, Φ_{nf}	0.001
Formation thickness, Δz, ft	250	Natural-fracture total compressibility, c_{nf}, psi^{-1}	2.5×10^{-4}
Reservoir depth, h, ft	5,800	Natural-fracture permeability, k_{nf}, md	1,600
Reservoir temperature, T, °F	200	Matrix total compressibility, c_{tm}, psi^{-1}	2.5×10^{-4}
Initial reservoir pressure, P_i, psi	3,800	Matrix permeability, k_m, md	3.2×10^{-5}
Horizontal well length, L_h, ft	4,800	Matrix porosity, Φ_m	0.05
Constant flowing bottomhole pressure, P_{wf}, psi	1,000	Viscosity, μ, cp	0.0184
Hydraulic-fracture number	10	Langmuir's volume, V_L, scf/ton	77.56
Distance between hydraulic fractures, 2_{ye}, ft	500	Langmuir's pressure, P_L, psi	2,285.7
Hydraulic-fracture porosity, Φ_{hf}	0.5	Non-Darcy-flow constant, β, ft^{-1}	1.29×10^{6}
Hydraulic-fracture total compressibility, c_{hf}, psi^{-1}	2.5×10^{-4}		
Hydraulic-fracture half-length, X_f, ft	250		

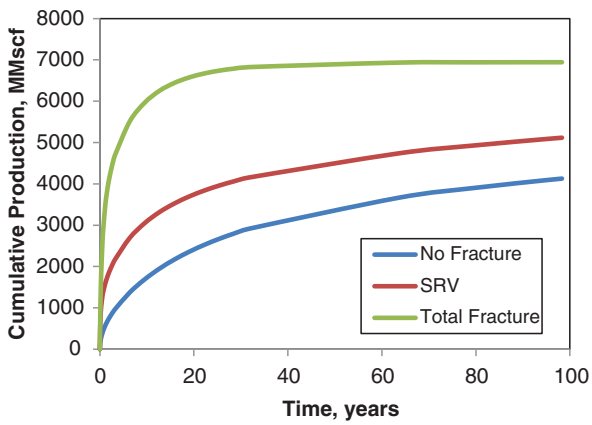

Fig. 13—Simulated gas-production performance for the three fracture models.

Fig. 13 compares the performance of the fractured horizontal well for the three fracture models. The comparison indicates that the fracture model makes a difference in well performance. The contribution from active natural fractures is evident and helps to yield higher production rates for a long period. A larger SRV leads to a higher gas-production rate.

For the second fracture model, pressure distributions at 1 year and 20 years are presented in **Fig. 14.**

Fig. 15 shows the cumulative-production comparison between cases with and without the Klinkenberg effect. Here, our simulator handles the Klinkenberg beta factor not as a constant value, but a changing value with matrix permeability and pressure. As shown in Table 2, the input data of matrix permeability are 3.2×10^{-5} md, and the initial reservoir pressure is 3,800 psi. With this permeability value and under higher pressure, the Klinkenberg effect will not have an obvious influence on gas-flow permeability on the basis of the estimation in Fig. 3. However, the constant bottomhole production pressure is set as 1,000 psi, which is much smaller than the reservoir initial pressure. When the pressure of the region near the wellbore and hydraulic fracture decreases quickly, the Klinkenberg effect becomes important for the flow in this region. On the basis of Eqs. 12 and 13, the effective permeability considering the Klinkenberg effect at initial pressure (3,800 psi) is 3.69×10^{-5} md, whereas that at bottomhole pressure (1,000 psi) is 5.0×10^{-5} md. Our simulation result in Fig. 15 also shows the influence of the Klinkenberg effect. It leads to approximately a 4% increase to the total gas production.

We studied the non-Darcy flow in the preceding scenario of a horizontal well with multistage hydraulic fractures and natural fractures to see its influence on gas production. The simulation result is shown in **Fig. 16 and 17.** The difference is observed on the gas cumulative production between the case considering the non-Darcy flow and the case not considering the non-Darcy flow in the first 6 years. Not considering the non-Darcy flow inside hydraulic fractures could lead to an overestimate of approximately 5% of cumulative gas production. After that, the difference between cases diminishes until these two curves coincide at approximately 40 years.

This simulation result is reasonable with the following analysis. In **Fig. 18,** we compare the calculated gas-flow velocities from Darcy's law and the Forchheimer equation for different pressure gradients. The parameters of permeability, viscosity, and the non-Darcy-flow factor in this calculation are the same as those in Table 2. When the pressure gradient is less than 1.0×10^{-3} psi/ft or velocity is less than10 ft/D, there is almost no difference between these two calculations. However, if the pressure gradient

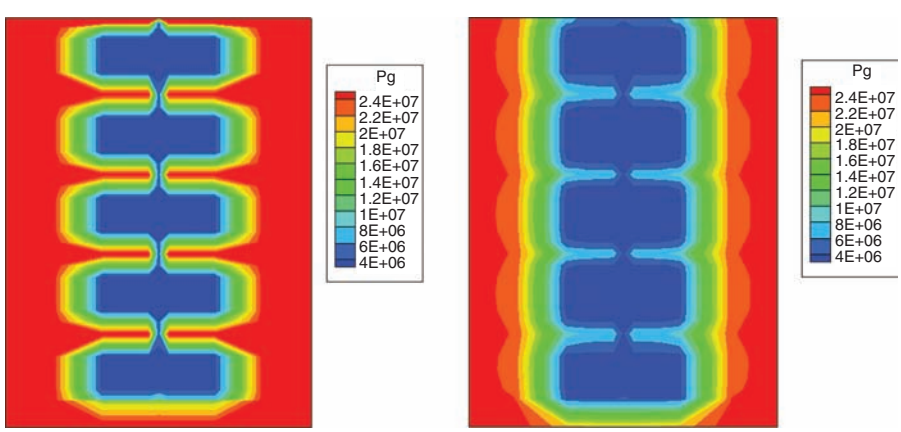

Fig. 14—Pressure distribution at 1 year (left) and 20 years (right) of Fracture Model #2 (unit: Pa).

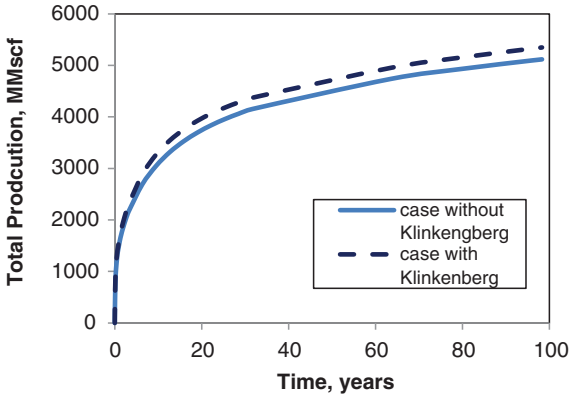

Fig. 15—Gas-cumulative-production behavior with the Klinkenberg effect.

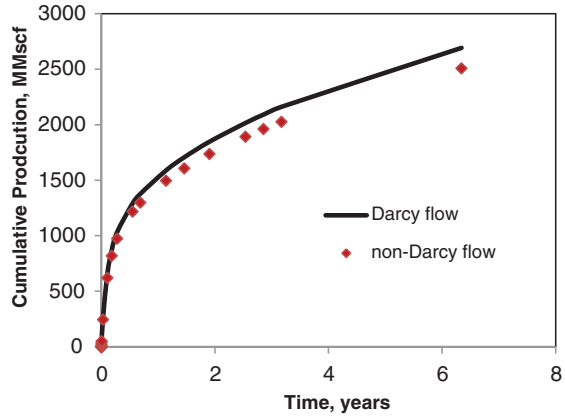

Fig. 16—Gas-cumulative-production behavior with non-Darcy flow in the first 6 years.

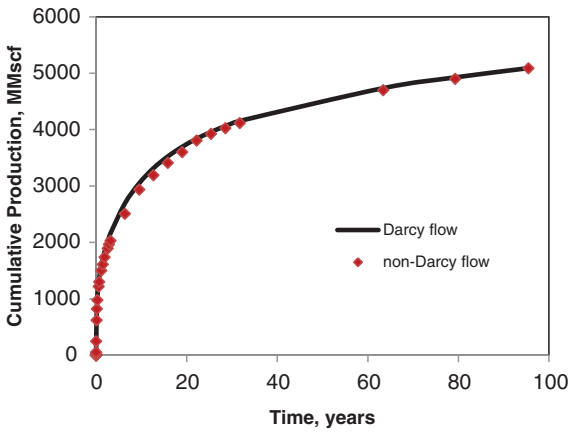

Fig. 17—Gas cumulative-production behavior with non-Darcy flow in 100 years.

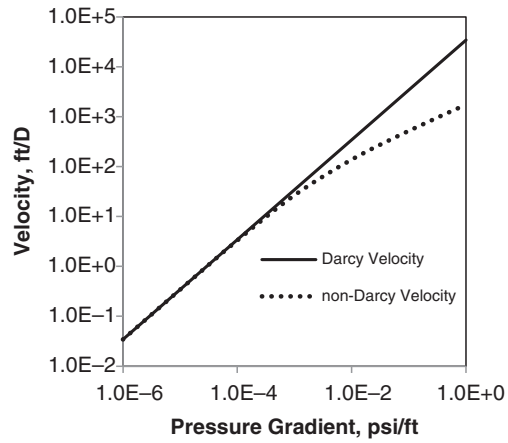

Fig. 18—Darcy and non-Darcy velocities with pressure gradient.

keeps increasing from 1.0×10^{-3} psi/ft, the difference will become larger. **Fig. 19** shows the calculated average gas flow rate inside hydraulic fractures with production time in the case that does not consider the non-Darcy flow. For the first 6 years, flow velocities locate in the range in which the difference between the Darcy flow and the non-Darcy flow is obvious. After that, flow velocities move to the area in which the difference is negligible.

Fig. 20 shows the simulated-well cumulative production vs. time with and without geomechanics effect. The relationship used for describing the effective stress and permeability of the unconventional reservoir is shown in Fig. 1, by use of a table-lookup input of the figure data. As shown in Fig. 20, geomechanics/flow coupling has a large impact on formation permeability, especially for the natural-fracture system. Consider the Muska formation, for example, when the effective stress increases from 1,600 to 4,800 psia and permeability decreases to 1/20 of its original value. With the gas production, reservoir effective stress increases as pore pressure decreases, leading to the large reduction of cumulative gas production.

Figs. 21 and 22 present the results for adsorption analysis with the numerical model. On the basis of the data in Table 2, we calculate the total gas mass as free gas in the micropores and

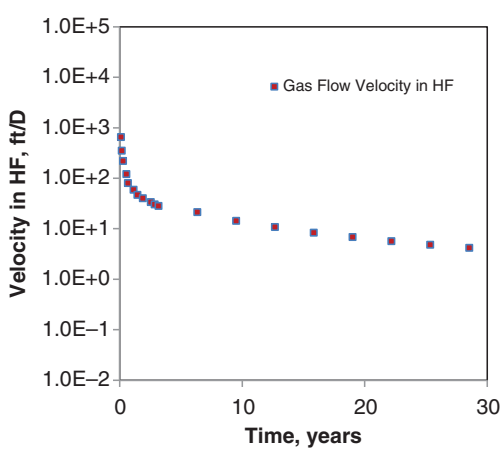

Fig. 19—Calculated gas-flow velocity with time in hydraulic fractures.

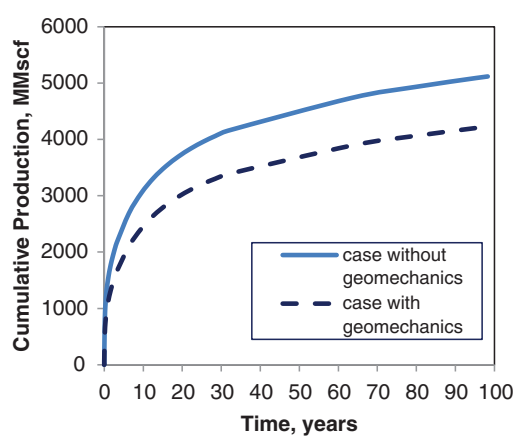

Fig. 20—Gas-cumulative-production behaviors with geomechanics.

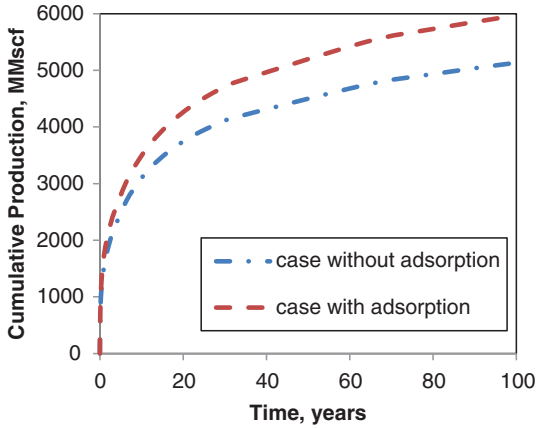

Fig. 21—Gas-cumulative-production behaviors with adsorption.

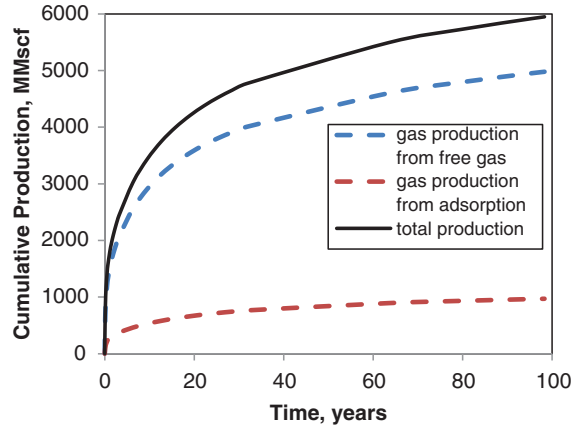

Fig. 22—Gas-production analysis from free gas and adsorbed gas.

adsorbed gas at initial condition. The proportion of gas stored in the pore space is approximately 77%, whereas that stored as adsorption is 23%. Then, we compare the cumulative gas production with and without considering adsorption. Simulation results (Fig. 21) show that the estimated gas production will increase with considering adsorption. This difference will become more and more evident. For the situation considering gas adsorption/desorption, gas production from the desorption is approximately 13%, and the produced portion of the free gas consists of 87%, as shown in Fig. 22.

Summary and Conclusions

This paper discusses a generalized-framework mathematical model for modeling gas production from unconventional gas reservoirs. The model formulation incorporates known nonlinear flow processes, associated with gas production from low-permeability unconventional reservoirs, including the Klinkenberg, non-Darcy-flow, and nonlinear-adsorption effects. The model formulation and numerical scheme are based on a generalized two-phase (gas/liquid) -flow model with unstructured grids. Specifically, a hybrid modeling approach is presented by combining discrete fracture, multidomain, and multicontinuum concepts for handling hydraulic fractures and a fracture network in SRV, distributed natural fractures, microfractures as well as porous matrix. We have verified the numerical models against analytical solutions for the Klinkenberg, non-Darcy-flow, and nonlinear-adsorption effects.

As application examples, we present modeling studies with three fracture models for gas production from a 10-stage hydraulic-fractured horizontal well, incorporating the Klinkenberg, non-Darcy-flow, and nonlinear-adsorption effects. The model results show that there is a large impact of various fracture models on gas-production rates as well as cumulative production.

Acknowledgments

This work was supported in part by EMG Research Center and UNGI of the Petroleum Engineering Department at Colorado School of Mines; by Foundation CMG; by RIPED of PetroChina Company; and by IFPEN.

References

Blasingame, T.A. 2008. The Characteristic Flow Behavior of Low-Permeability Reservoir Systems. Paper SPE 114168 presented at the SPE Unconventional Reservoirs Conference, Keystone, Colorado, 10–12 February. http://dx.doi.org/10.2118-MS.

Bustin, R.M., Bustin, A.M.M., Cui, X. et al. 2008. Impact of Shale Properties on Pore Structure and Storage Characteristics. Paper SPE 119892 presented at the SPE Gas Production Conference, Fort Worth, Texas, 16–18 November. http://dx.doi.org/10.2118/119892-MS.

Cipolla, C.L. 2009. Modeling Production and Evaluating Fracture Performance in Unconventional Gas Reservoirs. *J. Pet Tech* **61** (9): 84–90 (Distinguished Author Series). http://dx.doi.org/10.2118/118536-PA.

Cipolla, C.L., Lolon, E.P., Erdle, J.C. et al. 2010. Reservoir Modeling in Shale-Gas Reservoirs. *Res Eval & Eng*. **13** (4): 638–653. http://dx.doi.org/10.2118/125530-PA.

Cipolla, C.L., Warpinski, N.R., Mayerhofer, M.J. et al. 2009. The Relationship Between Fracture Complexity, Reservoir Properties, and Fracture Treatment Design. Paper SPE 115769 presented at the SPE ATC&E, Denver, Colorado, 21–24 September. http://dx.doi.org/10.2118/115769-MS.

Davies, J.P. and Davies, D.K. 1999. Stress-Dependent Permeability Characterization and Modeling. Paper SPE 56813 presented at the SPE ATCE, Houston, Texas, 3–6 October. http://dx.doi.org/10.2118/56813-MS.

EIA (US Energy Information Administration). 2011. World Shale Gas Resources: An Initial Assessment of 14 Regions Outside the United States (April).

Ertekin, T., King, G.R., and Schwerer, F.C. 1986. Dynamic Gas Slippage: A Unique Dual-Mechanism Approach to the Flow of Gas in Tight Formations. *SPE Form Eval* **1** (1): 43–52. http://dx.doi.org/10.2118/12045-PA.

Evans, R.D., and Civan, F. 1994. Characterization of Non-Darcy Multiphase Flow in Petroleum Bearing Formation. Final Report for US Department of Energy Assistant Secretary for Fossil Energy.

Forsyth, P.A., Wu, Y.S., and Pruess, K. 1995. Robust Numerical Methods for Saturated-Unsaturated Flow With Dry Initial Conditions in Heterogeneous Media. *Advance in Water Resources* **18:** 25–38.

Freeman, C.M., Moridis, G.J., Ilk, D. et al. 2010. A Numerical Study of Transport and Storage Effects for Tight Gas and Shale Gas Reservoir Systems. Paper SPE 131583 presented at the SPE International Oil and Gas Conference and Exhibition, Beijing, China, 8–10 June. http://dx.doi.org/10.2118/131583-MS.

Freeman, C.M., Moridis, G.J., and Blasingame, T.A. 2009a. A Numerical Study of Microscale Flow Behavior in Tight Gas and Shale Gas Reservoir Systems. *Proceedings of the 2010 TOUGH Symposium, Berkeley, California, 14–16 September*.

Freeman, C.M., Moridis, G.J., Ilk, D. et al. 2009b. A Numerical Study of Tight Gas and Shale Gas Reservoir Systems. Paper SPE 124961 presented at the SPE Annual Technical Conference and Exhibition, New Orleans, Louisiana, 4–9 October. http://dx.doi.org/10.2118/124961-MS.

Gao, C., Lee, J.W., Spivey, J.P. et al. 1994. Modeling Multilayer Gas Reservoirs Including Sorption Effects. Paper SPE 29173 presented at the SPE Eastern Regional Conference and Exhibition, Charleston, West Virginia, 8–10 November. http://dx.doi.org/10.2118/29173-MS.

Kelkar M. and Atiq, M. 2010. Upgrading Method for Tight Gas Reservoirs. Paper SPE 133301 presented at the SPE Annual Technical

Conference and Exhibition, Florence, Italy, 19–22. http://dx.doi.org/10.2118/133301-MS.

Klinkenberg, L.J. 1941. The Permeability of Porous Media to Liquids and Gases. In *API Drilling and Production Practice*, 200–213.

Langmuir, I. 1916. The Constitution and Fundamental Properties of Solids and Liquids. *J. Am. Chem. Soc.* **38** (11): 2221–2295.

Leahy-Dios, A., Das, M., Agarwal, A. et al. 2011. Modeling of Transport Phenomena and Multicomponent Sorption for Shale Gas and Coalbed Methane in an Unstructured Grid Simulator. Paper SPE 147352 presented at the SPE Annual Technical Conference, Denver, Colorado, 30 October–2 November. http://dx.doi.org/10.2118/147352-MS.

Leverett, M.C. 1941. Capillary Behavior in Porous Media. *Trans AIME* **142:** 341–358.

Li, J., Du, C.M., and Zhang, X. 2011. Critical Evaluation of Shale Gas Reservoir Simulation Approaches: Single-Porosity and Dual-Porosity Modeling. Paper presented at the SPE Middle East Unconventional Gas Conference and Exhibition, Muscal, Oman, 31 January–2 February.

Mengal, S.A. and Wattenbarger, R.A. 2011. Accounting for Adsorbed Gas in Shale Gas Reservoirs. Paper SPE 141085 presented at the SPE Middle East Oil and Gas Show and Conference, Manama, Bahrain, 25–28 September. http://dx.doi.org/10.2118/141085-MS.

Moridis, G.J., Blasingame, T.A., and Freeman, C.M. 2010. Analysis of Mechanisms of Flow in Fractured Tight-Gas and Shale-Gas Reservoirs. Paper SPE 139250 presented at the SPE Latin American and Caribbean Petroleum Engineering Conference, Lima, Peru, 1–3 December. http://dx.doi.org/10.2118/139250-MS.

Ozkan, E., Raghavan, R., and Apaydin, O.G. 2010. Modeling of Fluid Transfer From Shale Matrix to Fracture Network. Paper SPE 134830 presented at the SPE ATC&E, Florence, Italy, 19–22 September. http://dx.doi.org/10.2118/134830-MS.

Pruess, K. 1983. *GMINC*—A Mesh Generator for Flow Simulations in Fractured Reservoirs, Report LBL-15227, Berkeley, California: Lawrence Berkeley National Laboratory.

Pruess, K. and Narasimhan, T.N. 1985. A Practical Method for Modeling Fluid and Heat Flow in Fractured Porous Media. *Soc. Pet. Eng. J.* **25:** 14–26.

Pruess, K., Oldenburg, C., and Moridis, G. 1999. *TOUGH2 User's Guide, Version 2.0*, Report LBNL-43134, Berkeley, California: Lawrence Berkeley National Laboratory.

Rubin, B. 2010. Accurate Simulation of Non-Darcy Flow in Stimulated Fractured Shale Reservoirs. Paper SPE 132093 presented at the SPE Western Regional Meeting, Anaheim, California, 27–29 May. http://dx.doi.org/10.2118/132093-MS.

Rutqvist, J.Y.,Wu, S., Tsang, C.F. et al. 2002. A Modeling Approach for Analysis of Coupled Multiphase Fluid Flow, Heat Transfer, and Deformation in Fractured Porous Rock. *International J. Rock Mechanics and Mining Sci.* **39:** 429–442.

Silin, D. and Kneafsey, T. 2011. Gas Shale: From Nanometer-Scale Observations to Well Modeling. Paper CSUG/SPE 149489 presented at the Canadian Unconventional Resources Conference, Calgary, Alberta, Canada, 15–17 November. http://dx.doi.org/10.2118/149489-MS.

Soeder, D.J. 1988. Porosity and Permeability of Eastern Devonian Gas Shale. *SPE Form Eval* **3** (1): 116–124. http://dx.doi.org/10.2118/15213-PA.

Wang, F.P., Reed, R.M., Jackson, J.A. et al. 2009. Pore Networks and Fluid Flow in Gas Shales. Paper SPE 124253 presented at the SPE Annual Technical Conference and Exhibition, New Orleans, Louisiana, 4–7 October. http://dx.doi.org/10.2118/124253-MS.

Winterfeld, P.H. and Wu, Y.S. 2011. Parallel Simulation of CO_2 Sequestration With Rock Deformation in Saline Aquifers. Paper SPE 141514 prepared for presentation at the SPE Reservoir Simulation Symposium, The Woodlands, Texas, 21–23 February. http://dx.doi.org/10.2118/141514-MS.

Winterfeld, P.H. and Wu, Y.S. 2012. A Novel Fully Coupled Geomechanical Model for CO_2 Sequestration in Fractured and Porous Brine Aquifers. Paper presented at the XIX International Conference on Water Resources CMWR 2012, University of Illinois at Urbana-Champaign, Illinois, 17–22 June.

Wu, Y.S. 2002. Numerical Simulation of Single-Phase and Multiphase Non-Darcy Flow in Porous and Fractured Reservoirs. *Transport in Porous Media* **49:** 209–240.

Wu, Y.S. and Pruess, K. 2000. Integral Solutions for Transient Fluid Flow Through a Porous Medium With Pressure-Dependent Permeability. *International J. Rock Mechanics and Mining Sci.* **37:** 51–61.

Wu, Y.S., Pruess, K., and Persoff, P. 1998. Gas Flow in Porous Media With Klinkenberg Effects. *Transport in Porous Media* **32:** 117–137.

Wu, Y.S., Rutqvist, J., Karasaki, K. et al. 2008. A Mathematic Model for Rock Deformation Effect of Flow in Porous and Fractured Reservoirs. Paper ARMA-08-142 presented at the 42nd US Rock Mechanics Symposium and 2nd US–Canada Rock Mechanics Symposium, San Francisco, California, 29 June–2 July.

Wu, Y.S. and Wang, C. 2012. Transient Pressure Testing Analysis of Gas Wells in Unconventional Reservoirs. Paper SPE-SAS-312 presented at the SPE Annual Technical Symposium and Exhibition (ATS&E), Khobar, Saudi Arabia, 8–11 April.

Wu, Y.S., Wang, C., Li, J. et al. 2012. Transient Gas Flow in Unconventional Gas Reservoirs. Paper SPE 154448 presented at the EAGE Annual Conference and & Exhibition Incorporating SPE Europec, Copenhagen, Denmark, 4–7 June. http://dx.doi.org/10.2118/154448-MS.

Appendix A

Here, we derive the analytical solution for gas flow with adsorption/desorption. If the system is isothermal, the ideal-gas law applies, and the gravity effect is negligible, then gas flow in porous media with adsorption is described by the following equations:

$$\nabla \cdot (\rho v) = -\frac{\partial(\phi\rho + m_g)}{\partial t}, \quad \text{(A-1)}$$

where ρ is the gas density; v is the gas-flow velocity; ϕ is the porous-media porosity; m_g is the adsorbed gas mass in a unit formation volume at a given pressure; and t is the time.

According to the ideal-gas law,

$$PV = nRT \quad \text{(A-2)}$$

and

$$\rho = \frac{M}{RT}P = \beta P, \quad \text{(A-3)}$$

where M is gas molecular weight; R is the universal gas constant; β is a coefficient, for simplicity, defined as $\beta = \frac{M}{RT}$; and T is the system temperature.

From Darcy's law and the Langmuir isotherm (Eqs. 2 and 3),

$$v = -\frac{k}{\mu}\nabla P \quad \text{(A-4)}$$

and

$$m_g = \rho_R \rho_g V_E = \rho_R \rho_g V_L \frac{P}{P + P_L} = V\alpha \frac{P}{P + P_L}, \quad \text{(A-5)}$$

where ρ_R is rock bulk density; ρ_g is gas density at standard condition; V_E is the adsorption isotherm function for gas content; V_L is the Langmuir's volume in scf/ton; and P_L is Langmuir's pressure. α is a coefficient, for simplicity, defined as $\alpha = \rho_R \rho_g V_L$.

By substituting Eqs. A-4 and A-5 into Eq. A-1, we obtain

$$\nabla \cdot \left(\beta \frac{k}{\mu} P \nabla P\right) = \phi\beta \frac{\partial P}{\partial t} + \alpha \frac{\partial\left(\frac{P}{P + P_L}\right)}{\partial t}. \quad \text{(A-6)}$$

In radial coordinates,

$$\frac{1}{r}\frac{\partial}{\partial r}\left(r\frac{\partial P^2}{\partial r}\right) = \frac{2\phi\mu}{k}\frac{\partial P}{\partial t} + \frac{2\alpha\mu}{\beta k}\frac{\partial\left(\frac{P}{P + P_L}\right)}{\partial P}\frac{\partial P}{\partial t}, \quad \text{(A-7)}$$

$$\frac{1}{r}\frac{\partial}{\partial r}\left(r\frac{\partial P^2}{\partial r}\right) = \left[\frac{2\phi\mu}{k} + \frac{2\alpha\mu}{\beta k}\frac{P_L}{(P + P_L)^2}\right]\frac{\partial P}{\partial t}, \quad \text{(A-8)}$$

and

$$\frac{1}{r}\frac{\partial}{\partial r}\left(r\frac{\partial P^2}{\partial r}\right) = \left[\frac{\phi\mu}{Pk} + \frac{\alpha\mu}{P\beta k}\frac{P_L}{(P+P_L)^2}\right]\frac{\partial P^2}{\partial t}. \quad \ldots\ldots \text{(A-9)}$$

Eq. 9 becomes

$$\frac{1}{r}\frac{\partial}{\partial r}\left(r\frac{\partial P^2}{\partial r}\right) = \frac{1}{A}\frac{\partial P^2}{\partial t}, \quad \ldots\ldots\ldots\ldots\ldots\ldots\ldots \text{(A-10)}$$

where we define the coefficient

$$\frac{1}{A} = \frac{\phi\mu}{\overline{P}k} + \frac{\alpha\mu}{\overline{P}\beta k}\frac{P_L}{(\overline{P}+P_L)^2}. \quad \ldots\ldots\ldots\ldots\ldots\ldots \text{(A-11)}$$

We propose to use a history-dependent, constant, averaged pressure within the pressure-changed domain (Wu et al. 1998),

$$\overline{P} \approx \frac{\sum V_j P_j}{\sum V_j}, \quad \ldots\ldots\ldots\ldots\ldots\ldots\ldots\ldots \text{(A-12)}$$

where V_j is a controlled volume at the geometric center of which the pressure was P_j at the immediately preceding time when the solution was calculated. The summation, $\sum V_j$, is performed over all V_j in which pressure increases (or decreases) occurred at the preceding time value. P_j is always evaluated analytically at point j, on the basis of the previous estimated, constant diffusivity.

The well boundary proposed as a line source/sink well is

$$\lim_{x\to 0}\frac{\pi khr\beta}{\mu}\frac{\partial P^2}{\partial r} = Q_m. \quad \ldots\ldots\ldots\ldots\ldots\ldots\ldots \text{(A-13)}$$

Then, we could get a transient-pressure solution for gas flow with adsorption/desorption,

$$P^2(r,t) = P_i^2 - \frac{\mu Q_m}{2\pi khr\beta}Ei\left(-\frac{r^2}{4At}\right). \quad \ldots\ldots\ldots\ldots \text{(A-14)}$$

Yu-Shu Wu is a professor and Foundation CMG Research Chair in Petroleum Engineering at the Colorado School of Mines (CSM). He is also a guest scientist at the Earth Sciences Division of the Lawrence Berkeley National Laboratory (LBNL). Wu earned BS (Eqv.) and MS degrees in petroleum engineering in China, and MS and PhD degrees in reservoir engineering from the University of California at Berkeley. At CSM, he is teaching petroleum reservoir engineering courses, supervising graduate students, and conducting research in the areas of multiphase fluid and heat flow in porous media, enhanced oil recovery (EOR), CO_2 geosequestration and CO_2 EOR, reservoir simulation, enhanced geothermal systems, geomechanics coupling and rock-deformation effects, and unconventional hydrocarbon reservoirs. Previously, Wu was a staff scientist with LBNL for 14 years (1995 through 2008).

Jianfang Li is a senior research engineer at Research Institute of Petroleum Exploration and Development (RIPED), PetroChina. She earned BS and MS degrees in applied mathematics from Beijing University of Aeronautics and Astronautics and a PhD degree in reservoir engineering from the graduate school of RIPED. Li's research interests include optimization, algorithms for solving linear algebraic equations, reservoir simulation (carbonate-reservoir simulation, chemical-flooding reservoir simulation, natural-gas-reservoir simulation, and unconventional-hydrocarbon-reservoir simulation).

Didier-Yu Ding is a senior research engineer at IFP Energies Nouvelles in France. His research interests include numerical modeling and optimization, reservoir simulation and characterization, complex wells, and near-well flow. Ding holds a BS degree in mathematics from Peking University in China, and MS and PhD degrees in applied mathematics from University de Paris, France.

Cong Wang is a PhD candidate in petroleum engineering at CSM. He earned a BS degree from Peking University and an MS degree from the Petroleum Engineering Department, CSM. Wang's Master's degree study was on the development of an unconventional reservoir simulator and its application in transient-pressure analysis and fracture characterization. He has made several conference presentations at SPE events, and his current research involves fully coupling geomechanics and fluid flow in unconventional reservoirs.

Yuan Di is an associate professor in the Department of Energy and Resources Engineering, College of Engineering, Peking University. He earned a BS degree from Xi'an Jiaotong University, an MS degree from Xi'an University of Architecture and Technology, and a PhD degree from Tongji University, Shanghai—all in civil engineering. Di's research interests include the numerical simulation of multiphase flow in porous media, wave propagation in porous media, and the analysis of borehole stability.